Comparative Structure Analysis of Tyrosine and Valine Residues in Unprocessed Silk Fibroin (Silk I) and in the Processed Silk Fiber (Silk II) from *Bombyx mori* Using Solid-State ^{13}C,^{15}N, and ^{2}H NMR†

Tetsuo Asakura,* Rena Sugino, Juming Yao, Hidehiko Takashima, and Raghuvansh Kishore‡

Department of Biotechnology, Tokyo University of Agriculture and Technology, Koganei, Tokyo 184-8588, Japan

Received October 9, 2001

ABSTRACT: The solid-state ^{13}C CP-MAS NMR spectra of biosynthetically labeled [$^{13}C_\alpha$]Tyr, [$^{13}C_\beta$]Tyr, and [$^{13}C_\alpha$]Val silk fibroin samples of *Bombyx mori*, in silk I (the solid-state structure before spinning) and silk II (the solid-state structure after spinning) forms, have been examined to gain insight into the conformational preferences of the semicrystalline regions. To establish the relationship between the primary structure of *B. mori* silk fibroin and the "local" structure, the conformation-dependent ^{13}C chemical shift contour plots for Tyr C_α, Tyr C_β, and Val C_α carbons were generated from the atomic coordinates of high-resolution crystal structures of 40 proteins and their characteristic ^{13}C isotropic NMR chemical shifts. From comparison of the observed Tyr C_α and Tyr C_β chemical shifts with those predicted by the contour plots, there is strong evidence in favor of an antiparallel β-sheet structure of the Tyr residues in the silk fibroin fibers. On the other hand, Tyr residues take a random coil conformation in the fibroin film with a silk I form. The Val residues are likely to assume a structure similar to those of Tyr residues in silk fiber and film. Solid-state ^{2}H NMR measurements of [3,3-$^{2}H_2$]Tyr-labeled *B. mori* silk fibroin indicate that the local mobility of the backbone and the $C_\alpha-C_\beta$ bond is essentially "static" in both silk I and silk II forms. The orientation-dependent (i.e., parallel and perpendicular to the magnetic field) solid-state ^{15}N NMR spectra of biosynthetically labeled [^{15}N]Tyr and [^{15}N]Val silk fibers reveal the presence of highly oriented semicrystalline regions.

Silk, a fibrous protein produced by the domestic silkworm *Bombyx mori* (*B. mori*),[1] has a number of desirable properties, i.e., luster, comfort, high strength, and elasticity for textiles. In addition, recent studies clearly show that silk fibroin may find potential applications in the development and construction of various biotechnological and biomedical devices (*1*). In fact, the extensive use of the silk protein essentially originates from its unique amino acid composition translated into an unusual primary structure and hierarchical structural organization. The amino acid composition (in mol %) of *B. mori* fibrous protein showed the predominance of five amino acids: Gly (42.9%), Ala (30.0%), Ser (12.2%), Tyr (4.8%), and Val (2.5%) (*2*). Using the cDNA sequencing method, Mita et al. (*3*) and later Zhou et al. (*4*), employing shotgun sequencing strategy combined with traditional physical map-directed sequencing of the fibroin gene of the heavy chain, predicted the presence of unusual repeat sequences in the silk fibroin, shown in Figure 1. Their analysis revealed that the primary structure of *B. mori* silk fibroin may be approximately divided into four regions. The repetitive region R (i, ii, and iii) and amorphous region A (iv) appear alternatively along the chain: (i) highly repetitive GAGAGS sequences constituting the crystalline region, (ii) relatively less repetitive GAGAGY and/or GAGAGVGY sequences comprising semicrystalline regions containing mainly hydrophobic moieties, (iii) sequences similar to i plus an extension by AAS, and (iv) amorphous regions containing negatively charged, polar, bulky hydrophobic, and aromatic residues, for example, TGSSGFGPYVANGGYSGYEYAWSSESDFGT. The superior nature of silk fibroin, making it an excellent natural fiber, basically originates from the combination of these unique amino acid sequences translating them into higher order structures.

The two crystalline forms, silk I and silk II, are reported as dimorphs of silk fibroin on the basis of extensive investigations from X-ray fiber diffraction (*5*−*11*), electron diffraction (*8*, *9*, *11*), conformational energy calculations (*12*, *13*), infrared (*14*), and ^{13}C and ^{15}N solid-state NMR spectroscopy (*14*−*25*). The silk I form is the silk fibroin structure in the solid state before spinning, where the sample is obtained either as a film from liquid silk in the silk gland of the silkworm or as an aqueous solution of the regenerated silk fibroin. The silk II form is the structure after spinning

† This work was financially supported by the Program for Promotion of Basic Research Activities for Innovative Biosciences, Japan. The work was carried out partly under a JSPS Invitation Fellowship offered to R.K.

* To whom correspondence should be addressed. E-mail: asakura@cc.tuat.ac.jp.

‡ On leave from the Institute of Microbial Technology, Sector 39-A, Chandigarh-160 036, India.

[1] Abbreviations: *B. mori*, *Bombyx mori*; CP-MAS, cross-polarization−magic angle spinning; DNA, deoxyribonucleic acid; FID, free induction decay; Fmoc, 9-flourenylmethoxycarbonyl; HATU, *N*-[(dimethylamino)-1*H*-1,2,3-triazolo[4,5-*b*]pyridin-1-ylmethylene]-*N*-methylmethanaminium hexafluorophosphate *N*-oxide; NMR, nuclear magnetic resonance; PEG-PS, poly(ethylene glycol)−polytstyrene; ppm, parts per million; τ_c, motional correlation time; TMS, tetramethylsilane; TFA, trifluoroacetic acid.

10.1021/bi0119013 CCC: $22.00
Published on Web 03/05/2002

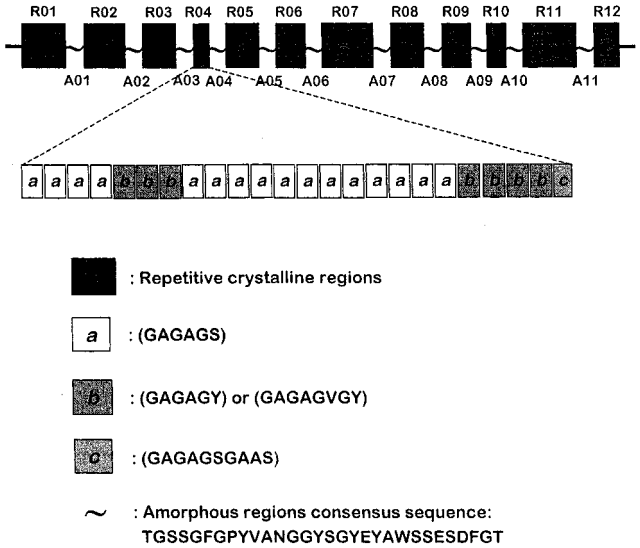

FIGURE 1: Schematic representation of the organization of the *B. mori* fibroin heavy chain gene. R01...R12 and A01...A11 represent the predicted 12 repetitive and 11 amorphous regions, respectively, in the polypeptide chain. An approximate amino acid sequence of the R04 region is illustrated by ***a***, ***b***, and ***c*** whereas the symbol ~ depicts a typical amino acid sequence in the amorphous region.

and is obtained as silk fibers from the cocoon after spinning. Numerous X-ray diffraction studies have reported the determination of the structure of silk II (*5*−*7*, *11*−*13*). The combined results of the analysis on the silk II structure, obtained from cocoons or as oriented silk rods prepared by stretching the liquid silk from silk glands, unambiguously established an antiparallel β-sheet structure.

Despite a long history of interest in the "less stable" silk I form, its structure has remained poorly understood, since any attempts to induce orientation of the silk I form for X-ray and electron diffractions studies easily cause its conversion into the more stable silk II form (*8*−*16*). Nevertheless, we recently characterized the molecular structure of silk I by using a synthetic peptide $(AG)_{15}$ as the model for the highly repetitive crystalline domain. We employed several solid-state NMR techniques and quantitative use of the ^{13}C CP-MAS NMR chemical shifts, in conjunction with the results obtained by molecular simulation studies (*24*). The existence of a repeated β-turn type II structure ($\phi_{Ala} \sim -60 \pm 5°$, $\psi_{Ala} \sim 130 \pm 5°$ and $\phi_{Gly} \sim 70 \pm 5°$, $\psi_{Gly} \sim 30 \pm 5°$) stabilized by a classical 4 → 1 *intra*molecular hydrogen bond was proposed for the silk I form. The overall planar sheets are held together by a number of *inter*molecular hydrogen-bonding interactions, involving the "central amide bond" of the β-turn, perpendicular to *intra*molecular interactions. It may be mentioned that it is possible to produce the silk I and/or silk II structural forms(s) of both silk fibroin and the derived peptides. Namely, if the silk fibroin sample or the $(AG)_{15}$ model peptide is dissolved in 9 M LiBr solution and dialyzed against distilled water, the resulting structure will be silk I, whereas any silk I sample treated with formic acid and dried will give predominantly silk II. These conversions were ascertained primarily by employing ^{13}C NMR spectroscopy and analyzing the peak shape and chemical shift values of the Ala C_α, Ala C_β, Ala C═O, and Gly C_α resonances.

There have been very limited studies on the sequences representing semicrystalline regions, although such sequences may critically contribute to many superiorities inherently associated with silk fibroin. For example, the presence of Tyr residues may be one of the origins providing solubility of silk fibroin in water (*25*). In general, it has been difficult to obtain detailed structural information for the semi-crystalline regions, mainly because of the lack of suitable analytical techniques required. The combined use of specific isotope labeling of silk fibroin and solid-state NMR, together with "selected" model peptides labeled suitably for NMR studies is a powerful approach to investigate the relationship between primary and secondary structures for such semi-crystalline domains. From the amino acid composition of the fibroin protein, the relative contents of Tyr (4.8%) and Val (2.5%) residues appear to be reasonably high, as they stand fourth and fifth behind Gly, Ala, and Ser (*2*−*4*). The primary structure indicates that these residues are largely located in the repetitive hexameric (-GAGAGY-) and octameric (-GAGAGVGY-) units of the semicrystalline regions. Consequently, the labeled Tyr and Val residues may be exploited not only to get insight but also to monitor the structural changes in the semicrystalline regions of the silk fibroin molecule. Previous solid-state ^{13}C and ^{15}N NMR studies of the fibroins have been very successful both for conformational characterization of highly ordered fibers and in distinguishing polymorphic forms of *B. mori* silk fibroin (*14*−*23*). For example, the observed isotropic chemical shifts are distinctly different between silk I, silk II, and α-helical structures (*14*−*17*, *21*, *26*). In addition, contour plots correlating the backbone torsion angles, ϕ and ψ, with the observed ^{13}C chemical shifts have been established for analyzing the conformational features (*27*). A comparison between the ^{13}C NMR chemical shifts and the backbone torsion angles in the form of contour plots has been used to determine the silk I structure (*21*, *24*, *26*).

The use of solid-state ^{13}C and ^{15}N NMR for the structural investigation of highly ordered fibrous systems has also been described (*18*, *23*). In our previous study, we reported the analysis of ^{15}N NMR spectra of *B. mori* silk fiber obtained from uniaxially aligned molecules placed with the axis of alignment both parallel and perpendicular to the magnetic field, B_0, to yield information on the local orientations of specific molecular bonds (*18*). The orientation-dependent nuclear spin interaction tensors serve as probes with which the orientations of specific bond vectors with respect to the fiber axis can be accurately determined. This possibility for determination of the backbone torsion angles, ϕ and ψ, of fibrous proteins by combined use of several bond vectors for specific ^{13}C or ^{15}N nuclei has been recently highlighted (*23*).

Solid-state ^{2}H NMR spectroscopy has also been a powerful tool to analyze the molecular motion and local structures of selectively deuterium-labeled macromolecules, i.e., fiberlike materials (*22*, *28*−*32*). The spectral line shape and relaxation behavior are largely determined by the orientation-dependent quadrupolar interaction (spin $I = 1$). The observed coupling between the deuterium quadrupole moment and the electric field gradient at the nucleus carries information about the spatial alignment and motional averaging of the labeled segment. ^{2}H NMR line shapes and relaxation times can thus be analyzed in terms of restricted anisotropic motions. It should be noted that the quadrupole echo experiments are generally applicable to the dynamic range of 10^{-8} s < τ_c <

Table 1: Characteristic ^{13}C NMR Chemical Shifts (in ppm from TMS) of Silk I [$(AG)_{15}$, Film] and Silk II [$(AG)_{15}$, Fiber] Samples and Natural Abundance Chemical Shifts of Peptides **1** and **2**

						models			
						peptide **1**[a]		peptide **2**[b]	
	liquid	silk I		silk II		9 M LiBr/	formic acid	9 M LiBr/	formic acid
residue	silk	$(AG)_{15}$	film	$(AG)_{15}$	fiber	dialysis	treatment	dialysis	treatment
Gly C_α	42.7	43.2	43.8	42.4	42.5	42.4	42.3	42.6	42.5
Gly C═O	171.3	169.9	170.7	169.1	169.3	169.2	169.1	169.4	169.3
Ala C_α	50.0	50.7	51.4	48.7	48.9	49.0	48.9	48.8	48.9
Ala C_β	16.6	16.5	16.5	16.7, 19.6, 22.2	16.6, 19.6, 21.9	17.0, 21.5	16.5, 21.3	16.8, 20.2	16.4, 20.5
Ala C═O	175.5	176.8	177.0	171.8	172.2	172.3	172.1	172.1	172.2
Ser C_α	55.9		58.0		54.6				
Ser C_β	61.3		60.7		63.9				
Ser C═O	172.4		173.7		*c*				
Tyr C_α	55.4		56 (br)[d]		54.2	53.7	53.8	≈54 (br)[d]	≈54 (br)[d]
Tyr C_β	36.1		36.0		40 (br)[d]	≈38 (br)[d]	≈38 (br)[d]	≈38 (br)[d]	≈38 (br)[d]
Tyr C═O	173.7					*e*	*e*	*e*	*e*
Val C_α	59.8		59 (br)[d]		56.9				

[a] $(AGYGAG)_5$. [b] $(AG)_3YGAGVGAGYG(AG)_3YG(AG)_3$. [c] Overlapped with Ala C═O. [d] br, broad peak. [e] Overlapped with the Ala C═O peak.

10^{-3} s, which covers a wide range of different molecular motions, such as diffusion processes, backbone dynamics, and aromatic side-chain ring flips (*30*−*32*).

In this paper, we first report the successful labeling of the Tyr and Val residues of native silk fibroin of *B. mori* for ^{13}C NMR studies, and we combine the use of ^{13}C CP-MAS NMR chemical shifts with a conformation-dependent chemical shift map, i.e., the contour plots, to analyze the labeled amino acids. The contour plots for the Tyr C_α, Tyr C_β, and Val C_α are constructed from the known ^{13}C chemical shift values in proteins with high-resolution crystal structures to evaluate the effect of conformation. To support the findings on labeled silk fibroin molecules, we also synthesized and analyzed the structure, by solid-state NMR, of two 30-mer model peptides: AGYGAGAGYGAGAGYGAGAGYGAGAGYGAG (**1**) and AGAGAGYGAGVGAGYGAGAGAGYGAGAGAG (**2**). While in peptide **1** the five Tyr residues are uniformly distributed in the $(AG)_{15}$ sequence, peptide **2** incorporates a single Val residue, in addition to three Tyr moieties. Furthermore, a ^2H NMR analysis of [3,3-$^2H_2$]Tyr-labeled silk fibroin, prepared as silk I and silk II forms, was performed to discuss the dynamics of the molecules. And last, the orientation dependence of ^{15}N NMR spectral line shapes of enriched [^{15}N]Tyr- and [^{15}N]Val-oriented silk fibers, prepared by culturing the silk gland, was also investigated. Such uniaxially oriented samples yield the spatial orientation of the labeled groups by means of a simple static wide-line experiment. A similar experiment was performed for [^{15}N]Ser-labeled oriented silk fibers. Since Ser residues are exclusively present in the repetitive crystalline domain of the $(\text{-GAGAGS-})_n$ sequence, this residue is a suitable reference for the well-oriented domain in the silk fiber.

MATERIALS AND METHODS

Preparation of Stable Isotope-Labeled Silk Fibroin. The ^{13}C-labeled amino acids [$^{13}C_\alpha$]Tyr, [$^{13}C_\beta$]Tyr, and [$^{13}C_\alpha$]Val (each 99% enrichment), used for labeling of silk fibroin, were purchased from Mastrace, Inc., Woburn, MA. The ^{15}N-labeled amino acids [^{15}N]Ser and [^{15}N]Val (both 99% enrichment) and [^{15}N]Tyr (99.7% enrichment) were purchased from Isotech Inc., Miamisburg, OH, and ICON, Mt. Marion, NY, respectively.

^{13}C labeling of *B. mori* silk fibroin was achieved biosynthetically by oral administration of an artificial diet with ^{13}C-enriched amino acids to larvae of the fifth instar (hybrids of Shuko and Rhuhaku), as reported previously (*33*). A representative example for the labeling of Tyr residues in *B. mori* silk fibroin is described here. Briefly, the supplementary Tyr was mixed with 2.7 g of an artificial diet per day. The amount of labeled Tyr was 10 mg on the fourth day and 15 mg each on the fifth and sixth day of the fifth larval stage. Thus, the total amount of Tyr was 40 mg per silkworm. The [$^{13}C_\alpha$]Tyr- and [$^{13}C_\beta$]Tyr-labeled silk fibroins enriched with [$^{13}C_\alpha$]Tyr and [$^{13}C_\beta$]Tyr residues, respectively, were isolated and confirmed by ^{13}C CP-MAS NMR spectra. A similar method was used to prepare [$^{13}C_\alpha$]Val-labeled silk fibroin. The [3,3-$^2H_2$]Tyr-labeled silk fibroin samples were obtained by oral administration of an artificial diet containing pertinent enriched amino acid during the fifth instar larval stage, as described previously (*31*).

Because of the high activity of transaminations in silkworms, the ^{15}N enrichment tends to be low when the oral administration method was used (*33*). Therefore, an improved isotopic labeling of the [^{15}N]Tyr, [^{15}N]Val, and [^{15}N]Ser residues in the fibroin molecules was achieved by culturing of *B. mori* posterior silk glands from 4-day-old, fifth instar larvae. This *in vitro* method has been developed in our laboratory, and details have been reported elsewhere (*33*). A large amount of silk fibroin (31 mg/g wet weight of the posterior silk gland, after 24 h culture) was produced using a rotation culture procedure with modified Grace's insect medium, containing pertinent ^{15}N-labeled amino acids, while bubbling oxygen gas through the medium.

The silk fibroin, stored in silk glands after the cultivation, was immersed in 30% cold ethanol for 12 h, and the pure silk fibroin was collected by the removal of swelled tissues and washing it repeatedly with 50% ethanol in a supersonic wave washer. After immersing it in dilute acetic acid, the silk sample was stretched 5-fold in length of the original sample. The oriented silk samples with aligned fibers were prepared as a block as detailed previously (*18*, *23*).

The two different structural forms of the native silk fibroin (silk I and silk II), referred to in Table 1 as "film" and "fiber", are routinely prepared in our laboratory, as described elsewhere (*14*, *15*). Briefly, to obtain the fibers, silk fibroin

was collected from *B. mori* cocoon pieces after removing the sericin protein by degumming it twice with 0.5 w/v % Marseilles soap solution at 100 °C for about 30 min and washing it thoroughly with distilled water (*14*). The fibers thus obtained were used directly for the analysis. To obtain the film, frequently referred as regenerated silk (*14*), the silk fibroin was treated with 9 M LiBr solution separately, and after extensive dialysis against distilled water the clear solution was dried gently at room temperature for several hours.

Peptide Synthesis. Fmoc amino acids and all reagents used in peptide synthesis were procured from PerSeptive Biosystems, Warrington, U.K. The resin and HATU were from Applied Biosystems and PE Biosystems, respectively. The solvents of high-purity grade and other chemicals were available locally from Wako Pure Chemical Industries Ltd.

The two model peptides, **1** and **2**, were synthesized by solid-phase Fmoc chemistry on a fully automated Pioneer peptide synthesis system (*24*). The peptide was assembled on Fmoc-Gly-PEG-PS resin (0.19 mmol/g). The coupling of Fmoc amino acids were performed by HATU. After synthesis, the free peptides were released from the resin by treatment with a 40 mL mixture of TFA, phenol, triisopropylsilane, and water (88:5:2:5 vol %) for 2 h at room temperature. The crude peptide was precipitated and washed repeatedly with cold diethyl ether. The precipitate, collected by centrifugation, was dried in a vacuum, dissolved in 9 M LiBr, and dialyzed extensively against distilled water. The desired peptide was recovered by filtration and/or lyophilization. This is a widely accepted method for the preparation of *B. mori* silk fibroin with silk I structure (*14*, *15*). To transform this structural form to silk II, the peptide was dissolved in a minimum amount of formic acid and dried at ambient temperature (*34*). In addition, the fraction of *B. mori* silk fibroin precipitated after chymotrypsin enzymatic cleavage (Cp fraction) was obtained with a silk I form, according to the method described earlier (*35*). The silk I structure of the Cp fraction was converted to the silk II form by formic acid treatment.

NMR Spectroscopy. ^{13}C CP-MAS NMR measurements were conducted on a Chemagnetics CMX-400 spectrometer operating at 100 MHz for ^{13}C. CP was employed for sensitivity enhancement with high-power ^{1}H decoupling during the signal acquisition interval. A ^{1}H 90° pulse width of 3 μs duration was used with a 1 ms contact time and a 3 s repetition time. Approximately 15K FIDs were added to generate the spectra. The chemical shifts were represented in parts per million with respect to the external reference adamantane. For direct comparison with previous data (*14*−*17*, *21*, *26*), we added 28.8 ppm to the observed chemical shifts to account for TMS as a reference on the silk I and silk II as well as the solution chemical shift data of the silk fibroins. The revised chemical shift values for the $(AG)_{15}$ sample of our previous work (*24*) are also listed in Table 1.

^{2}H NMR measurements were made on a 61.06 MHz Chemagnetics CMX Infinity 400 spectrometer equipped with suitable accessories. The details of the pulse sequence used have been described elsewhere (*31*, *32*). The spectral width was 2000 kHz, 8192 data points were collected, and the spectra represent 8K−10K scans acquired at room temperature. Lorentzian line broadening of 4 kHz was applied. For the line-shape analysis the MXQET program was used to simulate quadrupole echo ^{2}H NMR powder spectra as a function of the exchange rate and libration angle according to a suitable dynamic model, as previously described (*31*, *32*).

The solid-state ^{15}N NMR measurements were performed at 25 °C on a JEOL GX400 spectrometer operating at 40.4 MHz equipped with a probe of 7 mm inner diameter. A contact time of 3 ms and a repetition time of 5 s were used to accumulate a total of 5K−20K scans at room temperature. $^{15}NH_4NO_3$ was used as an external reference. The ^{15}N solution NMR spectra were observed with a JEOL FX-90Q NMR spectrometer operating at an ambient temperature. Cross-polarization with high-power ^{1}H decoupling was employed as described (*36*).

Preparation of ^{13}C Chemical Shift Contour Maps. Contour plots of the conformation-dependent chemical shifts of the Tyr C_α, Tyr C_β, and Val C_α carbons were generated from the known chemical shift data of 40 proteins whose X-ray coordinates were available from the Brookhaven Protein Data Bank. The relevant information about the proteins with their PDB codes has been provided in our previous publications (*27*). The conformation-dependent secondary shift ($\Delta\delta = \delta^{\text{observed}} - \delta^{\text{random}}$) is defined as the difference between the observed ^{13}C NMR chemical shift and the shift of the corresponding residues in the random/unordered structures. Such random coil chemical shift values were taken from the chemical shifts of the corresponding amino acid residues in *B. mori* silk fibroin in aqueous solution (*37*): 55.4 ppm for Tyr C_α, 36.1 ppm for Tyr C_β, and 59.8 ppm for Val C_α. The steps involved in the construction of the contour maps have been described in another paper (*27*).

RESULTS

Solid-State ^{13}C CP-MAS NMR Spectra of [$^{13}C_\alpha$]Tyr-, [$^{13}C_\beta$]-Tyr-, and [$^{13}C_\alpha$]Val-Labeled Silk Fibroins. The ^{13}C CP-MAS NMR spectra of native *B. mori* silk fibroin (i.e., nonlabeled) and of silk fibroin enriched with ^{13}C at the Tyr C_α (or [2-^{13}C]-Tyr),Tyr C_β (or [3-^{13}C]Tyr), and Val C_α (or [2-^{13}C]Val) sites are shown in Figures 2 and 3 for both the silk I (film) and silk II (fiber) forms, respectively. Only the expanded spectra between 10 and 70 ppm are shown, and the observed chemical shifts are summarized in Table 1. For the sake of comparison, the solution-state ^{13}C NMR chemical shifts of the silk fibroin have also been tabulated along with the ^{13}C isotropic chemical shifts from the CP-MAS experiments. By comparison of spectra **b**, **c**, and **d** with that of the nonlabeled material, **a**, the relatively increased peaks are assigned to the labeled carbons. To confirm these resonances, the spectrum of the native *B. mori* silk fibroin recorded under similar conditions was subtracted. As expected, the resulting difference spectra in Figure 4 contain the resonances arising predominantly from the labeled sites, while only small peaks in spectrum **a** are due to differences in the line shapes of the labeled and nonlabeled materials. Therefore, it is evident that the biosynthetic labeling technique described here successfully targets the C_α- and C_β-labeled sites of the Tyr residues in the silk fibroin and may be extended to other related biological model systems. Characteristic solid-state ^{13}C NMR chemical shifts of the Tyr C_α carbon are ∼56 and 54.2 ppm for film and fiber, respectively, and for Tyr C_β ∼36.0 and 40 ppm.

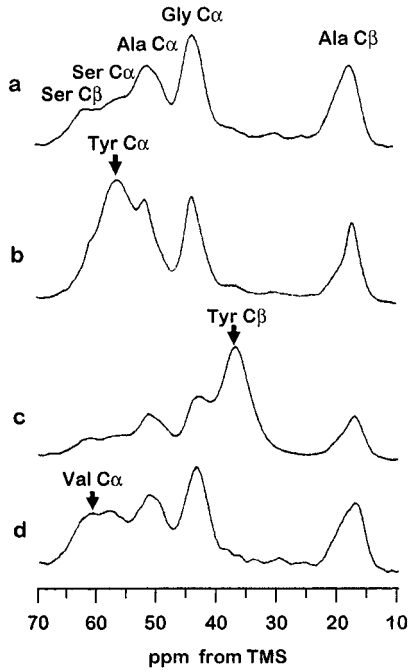

FIGURE 2: Solid-state ^{13}C CP-MAS NMR spectra (10−70 ppm) of *B. mori* silk fibroin with the silk I form (**a**) in its native state, i.e., unlabeled sample, (**b**) enriched with ^{13}C at the C_α site of the tyrosine residues, (**c**) enriched with ^{13}C at the C_β site of the tyrosine residues, and (**d**) enriched with ^{13}C at the C_α site of the valine residues.

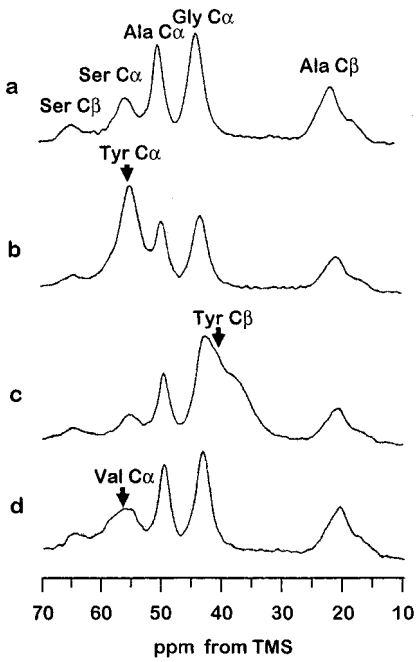

FIGURE 3: Solid-state^{13}C CP-MAS NMR spectra (30−70 ppm) of *B. mori* silk fibroin with the silk II form (**a**) in its native state, i.e., unlabeled sample, (**b**) enriched with ^{13}C at the C_α site of the tyrosine residues, (**c**) enriched with ^{13}C at the C_β site of the tyrosine residues, and (**d**) enriched with ^{13}C at the C_α site of the valine residues.

Figures 2**d** and 3**d** also show the ^{13}C CP-MAS spectra of the *B. mori* silk fibroin that has been enriched at the C_α site of Val. To ascertain that the assigned resonances (∼59 and 56.9 ppm for film and fiber, respectively) arise from the isotropically enriched Val C_α sites, again the spectrum of the nonlabeled native *B. mori* silk fibroin sample was

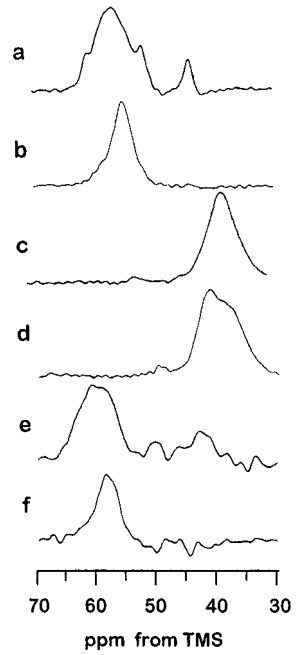

FIGURE 4: Solid-state ^{13}C CP-MAS NMR difference spectra (10−70 ppm) of labeled *B. mori* silk fibroins with the silk I (**a**, **c**, **e**) and silk II (**b**, **d**, **f**) structural forms: spectra **a** and **b** are the C_α sites of the tyrosine residues; spectra **c** and **d** are the C_β sites of the tyrosine residues, and spectra **e** and **f** represent the C_α sites of the valine residues.

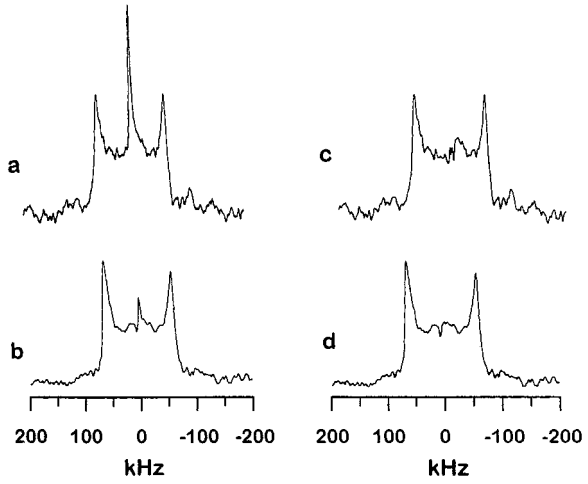

FIGURE 5: Solid-state ^{2}H NMR spectra (−200−200 ppm) of [3,3-$^{2}H_2$]Tyr-labeled *B. mori* silk fibroin with the silk I (**a** and **c**) and silk II (**b** and **d**) structural forms. Spectra **c** and **d** represent results after the water peak at the center is subtracted.

subtracted from the spectrum of the corresponding labeled sample. The difference NMR spectra of the silk I and silk II structural forms (Figure 4) clearly indicate that the labeling technique has successfully targeted the Val residues, too. From these results it appears that in solid state the Tyr C_α, Tyr C_β, and Val C_α resonances are conformationally sensitive.

Solid-State ^{2}H NMR Spectra of [3,3-$^{2}H_2$]Tyr-Labeled Silk Fibroins. We examined the solid-state ^{2}H NMR spectra of [3,3-$^{2}H_2$]Tyr-labeled silk fibroin in Figure 5 in the silk I (film) and silk II (fiber) structural forms. The observed line shapes could be satisfactorily simulated with an asymmetry parameter of $\eta = 0.00$ and a quadrupole coupling constant

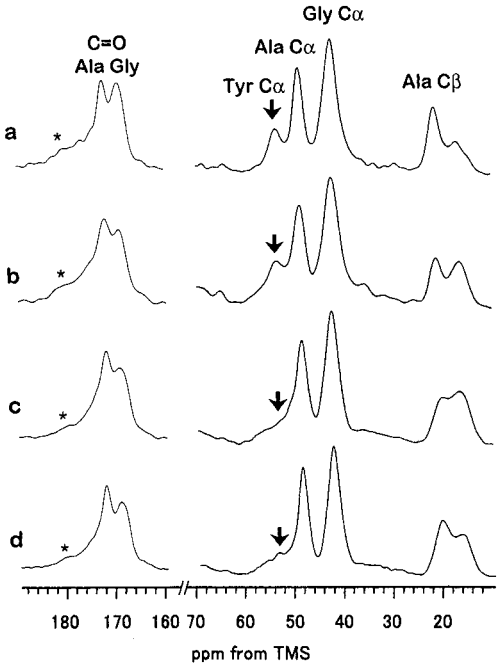

FIGURE 6: Solid-state ^{13}C CP-MAS NMR spectra (10−70 ppm and 160−190 ppm) of the two model peptides, **1** (**a**, **b**) and **2** (**c**, **d**). Spectra **a** and **c** were obtained after LiBr treatment and dialysis against distilled water for **1** and **2**, respectively. Spectra **b** and **d** were obtained after formic acid treatment for **1** and **2**, respectively. For both peptides the characteristic doublets of the Ala C_β resonances are clearly seen. The broad appearance of the Tyr C_α resonance in **2** is indicated by an arrow.

of Qcc = 164 kHz (*31*). On the basis of the model of a three-site jump around the $C_\alpha-C_\beta$ bond, a very slow rate constant of 10^3 Hz was obtained as reported previously for [3,3-$^2H_2$]-Tyr-labeled silk fibroin in the silk II form (*31*). Thus, the rotation about the $C_\alpha-C_\beta$ bond of the Tyr residues can be considered as essentially "static" for both of the samples. Therefore, we suggest that in *B. mori* silk fibroin the origin of the peak broadening may be due to the distribution of the "local" structural environment of the ^{13}C-labeled Tyr nuclei, presumably associated with multiple secondary structures of Tyr. We attribute a similar explanation also to the observed broad peaks of the Val C_α resonance.

*Sold-State ^{13}C CP-MAS NMR Spectra of Model Peptides **1** and **2***. Two model peptides, **1** and **2**, were synthesized to examine the influence of the presence of Tyr and Val residues on the structure of the $(Ala-Gly)_{15}$ sequence. Such information is usually difficult to obtain directly from silk fibroin samples. The solid-state ^{13}C CP-MAS NMR spectra of these peptides, after dissolution in 9 M LiBr solution and extensive dialysis against water, are shown in Figure 6, and the characteristic chemical shifts are summarized in Table 1, along with formic acid-treated samples. The resonance assignments of the constituent amino acids could be readily made from their relative peak area and by comparison with the spectra reported previously for several related silk fibroin model peptides (*25*). Both peptides gave remarkably similar ^{13}C chemical shifts; however, a marked difference in the relative intensities of the conformationally sensitive Ala C_β resonance (∼16.5 and ∼21.0 ppm) was apparent. It should be noted that the 9 M LiBr-treated $(AG)_{15}$ sequence yields a single sharp peak at ∼16.5 ppm for the Ala C_β resonance which could be assigned *exclusively* to the silk I structural form (*14*−*16*). Thus, the observed chemical shifts and the relative peak intensities of the Ala, Gly, and Tyr residues in **1** and the Ala, Gly, Tyr, and Val residues in **2** clearly indicate that both peptides assume a fiberlike silk II conformation rather than silk I, even after LiBr treatment, according to the summarized values in Table 1. The Tyr residues exhibit a dramatic destabilizing effect on the silk I structure, as judged from the characteristic doubling of the Ala C_β resonance at ∼16.5 and ∼21.0 ppm representing silk I and silk II, respectively. Of particular interest is the finding that the Tyr C_α resonance at 53.8 ppm (marked by arrow in peptide **1**) is closer to the fibrous form, which may be characteristic of predominantly β-sheet structures. The Tyr C_β peaks at ∼38 ppm remain significantly broadened. A careful interpretation of the results, in conjunction with the appearance of broad peaks for the Ala C_β and Ala carbonyl carbons at ∼16.5 and ∼177 ppm (marked by an asterisk), respectively, may suggest the existence of diverse structural forms of a "distorted β-turn" type (unpublished results). This interpretation is fully consistent with our recent proposal, based on experimental NMR as well as theoretical molecular simulation structural characterizations, of a "heterogeneous" structure of the silk II form. Further, the analysis of NMR spectra of **2** suggests that the presence of a single Val residue, as such, may not have any dramatic influence, particularly when it coexists with almost uniformly distributed Tyr residues. The simultaneous appearance of the characteristic silk II resonances in both **1** and **2**, as also analyzed from the split patterns of the Ala C_β resonance, provides evidence that these residues stabilize the silk II structure, i.e., an antiparallel β-sheet. The overall results on the model peptides clearly show that the effect of the Val residue is significant and nonnegligible. The present data, however, do not allow a quantitative evaluation of the destabilizing and stabilizing effects on the silk I and silk II structures, respectively, exerted by these two residues.

^{13}C NMR Chemical Shift Contour Maps of Tyr and Val Residues. Figures 7 and 8 show the contour plots of the conformation-dependent ^{13}C chemical shifts of the Tyr C_α and C_β carbons, respectively. The $\Delta(\phi, \psi)$ values in the left half of the Ramachandran map (i.e., $-180° < \phi < 0°$ and $-180° < \psi < 180°$) are reported. The analysis shows that indeed there exists a conformation dependence of the chemical shifts. For example, the chemical shifts falling in the helical region ($\phi \sim -57 \pm 20°$; $\psi \sim -47 \pm 20°$) of the ϕ, ψ map appear at much lower field (∼58.0 ppm) for the Tyr C_α resonance than those values (∼53.5 ppm) appearing in the β-sheet region ($\phi \sim -139 \pm 20°$; $\psi \sim 135 \pm 20°$). Interestingly, a reverse trend was observed for the Tyr C_β resonance, i.e., upfield chemical shifts for the helical region (∼35.5 ppm) and downfield shifts (∼38.5 ppm) for the extended β-sheet region. The Tyr carbon chemical shifts of silk fiber in the silk II form are examined in the contour plots in Figures 7 and 8. The observed chemical shifts, 54.2 ppm (Tyr C_α) and ∼40 ppm (Tyr C_β) are marked by assuming an error in the chemical shifts of ±0.5 ppm. The overlapped ϕ and ψ region, which satisfies both the Tyr C_α and Tyr C_β chemical shifts of silk fibers simultaneously, is located close to an extended β-sheet region in the Ramachandran map.

There are several areas which satisfy both the Tyr C_α and C_β chemical shifts of the silk film with silk I form. The

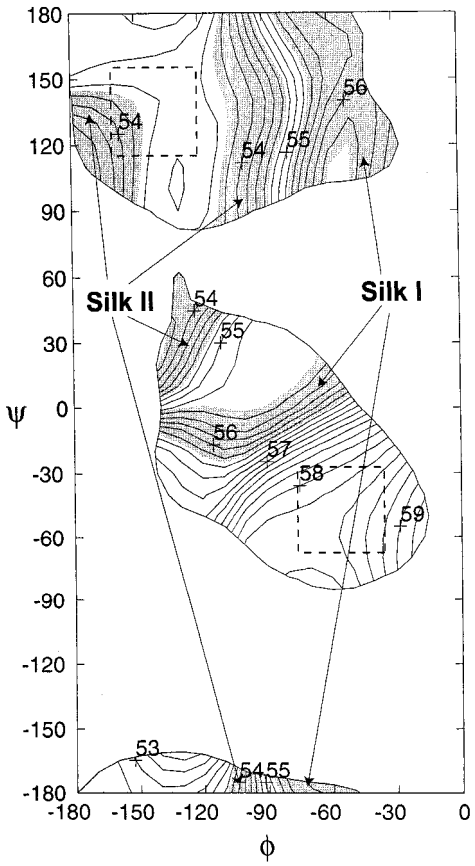

FIGURE 7: Contour plot of the conformation-dependent ^{13}C chemical shifts (in ppm) for the C_α carbon of Tyr residues in 40 proteins, shown as a function of torsion angles ϕ and ψ. Chemical shift values in the region $-180° < \phi < 0°$ and $-180° < \psi < 180°$ are shown where the density function is >1. The random coil chemical shift for the Tyr C_α carbon considered is 55.4 ppm. The areas of silk I chemical shift (56.0 ± 0.5 ppm) and of silk II chemical shift (54.2 ± 0.5 ppm) are shown in gray. The boxes with broken lines indicate α-helical (lower) and β-sheet (upper) regions.

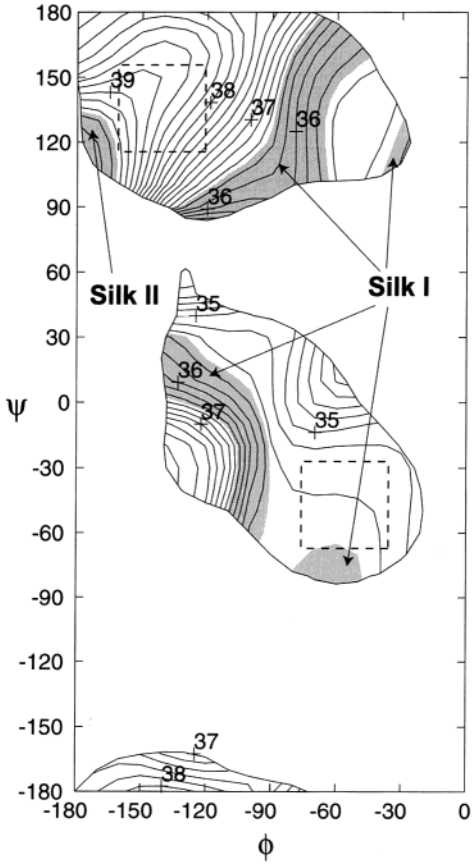

FIGURE 8: Contour plots of the conformation-dependent ^{13}C chemical shifts (in ppm) for the C_β carbon of Tyr residues in 40 proteins, shown as a function of torsion angles ϕ and ψ. Chemical shift values in the region $-180° < \phi < 0°$ and $-180° < \psi < 180°$ are shown where the density function is >1. The random coil chemical shift for the Tyr C_β carbon considered is 36.1 ppm. The areas of silk I chemical shift (36.0 ± 0.5 ppm) and of silk II chemical shift (40.0 ± 0.5 ppm) are shown in gray. The boxes with broken lines indicate α-helical (lower) and β-sheet (upper) regions.

chemical shifts are the same as those in liquid silk, but in the latter case there is a rapid exchange among various conformations on the NMR time scale. However, in the solid state the ^2H NMR analysis of [3,3-$^2H_2$]Tyr-labeled silk fibroin in the silk I form has shown that there is no interconversion among different conformations. Thus, it is likely that the Tyr residues assume several torsion angles in the silk film with the silk I form.

A similar conformation-dependent contour plot was constructed from the ^{13}C chemical shift values of the Val C_α carbon of known protein structures, as shown in Figure 9. The results indicate that the torsion angles, ϕ and ψ, exert a significant effect on the chemical shift values of the Val C_α carbons. The typical chemical shift values for α-helices are ~63.0 ppm (shift to lower field) and ~58.0 ppm (shift to higher field) for antiparallel β-sheets. A comparison of the observed ^{13}C chemical shifts of the Val C_α carbons with the contour map suggests that the most likely conformation for the Val residues in *B. mori* silk fiber (silk II form) is the extended β-sheet. On the other hand, we speculate that the Val residues in the silk film (silk I form) take several conformations that satisfy the chemical shift constraints, just as in the case of the Tyr residues in silk film.

Solid-State ^{15}N NMR Spectra of Oriented Silk Fibroin Fibers. Figure 10 shows the ^{15}N NMR spectra of [^{15}N]Tyr- and [^{15}N]Val-labeled *B.* mori silk fibroins in aqueous solution, along with the spectrum of [^{15}N]Ser-labeled fibroin (*33*). For comparison, the natural abundance ^{15}N NMR spectrum (lower most) of the native *B. mori* silk fibroin, obtained under similar conditions, is also shown. In the spectrum of each silk fibroin-labeled sample, only one major ^{15}N resonance is observed. The small peaks in the NMR spectra are attributed to the natural abundance in the samples. It should be mentioned that the nitrogen nuclei of the amide bonds in proteins, as donors, frequently participate in diverse hydrogen-bonding interactions in different secondary structures, along with other long-range interactions. A wide distribution of the shifts in the native silk fibroin may indicate that these moieties are likely to be distributed in different conformational states. We observed relatively low enrichment of [^{15}N]Val silk fibroin samples which could be due to low contents of the Val residues in the silk fibroin molecules; however, the intensity of the peak is still significant to the extent that the sample can be exploited for the solid-state NMR analysis. Thus, the results demonstrate that isotopic labeling of selected residues during the cultivation of the posterior silk gland of *B. mori* silk fibroin can yield

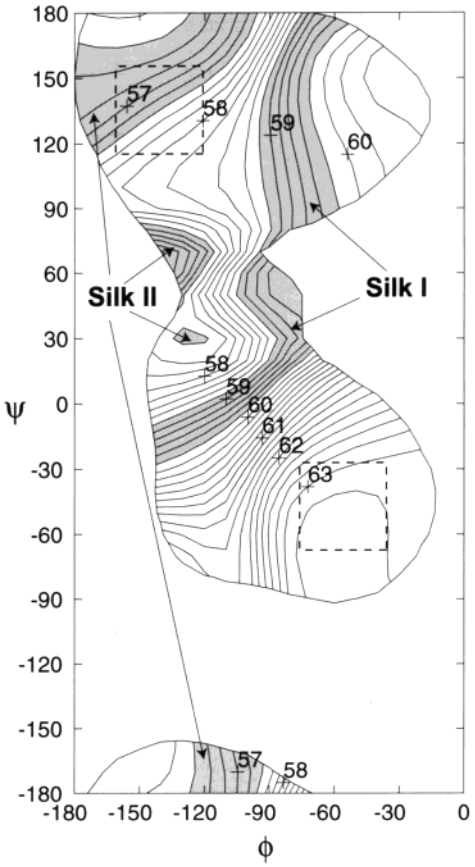

FIGURE 9: Contour plots of the conformation-dependent ^{13}C chemical shifts (in ppm) for the C_α carbon of Val residues in 40 proteins, shown as a function of torsion angles ϕ and ψ. Chemical shift values in the region $-180° < \phi < 0°$ and $-180° < \psi < 180°$ are shown where the density function is >1. The random coil chemical shift for the Val C_α carbon is considered 59.8 ppm. The areas of the silk I chemical shift (59.0 ± 0.5 ppm) and the silk II chemical shift (56.9 ± 0.5 ppm) are shown in gray. The boxes with broken lines indicate α-helical (lower) and β-sheet (upper) regions.

high ^{15}N incorporation for these three residues. This approach may be useful for the preparation of other related ^{15}N-labeled biomaterials in their native forms for structural investigations.

To gain insight into the structural organization of the fibroin molecules, we investigated the ^{15}N spectra of [^{15}N]Tyr, [^{15}N]Val, and [^{15}N]Ser silk fibers in the silk II forms in the solid state. Oriented samples were obtained as a block, which was placed with the fiber axis either parallel or perpendicular to the applied magnetic field (Figure 11). All of the experimental spectra were found to contain a contribution of approximately 30% of a nonoriented powder pattern which was subtracted from the observed spectra (*18*, *23*). The resulting spectral patterns in Figure 11 show significant differences between the parallel and perpendicular alignments, indicating that the Tyr and Val sites are well oriented within the macroscopic fiber. Since the spectral patterns are very similar to those of [^{15}N]Gly- and [^{15}N]Ala-labeled silk fiber samples reported previously, we conclude that the long silk fibroin chain represents an antiparallel β-sheet structure. Thus, most of the Tyr and Val sites, incorporated into the semicrystalline domains of repeated -GAGAGS- sequences, are suggested to assume the silk II structure.

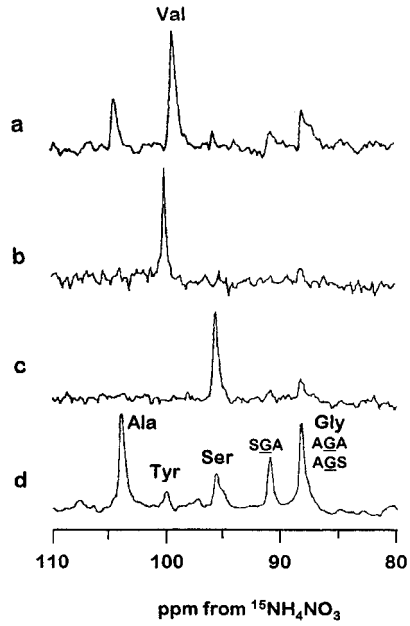

FIGURE 10: ^{15}N NMR solution spectra (80−110 ppm) of selectively labeled *B. mori* silk fibroin samples: (**a**) [^{15}N]Val silk fibroin, (**b**) [^{15}N]Tyr silk fibroin, and (**c**) [^{15}N]Ser silk fibroin. For comparison, the ^{15}N NMR spectrum (**d**) of an unlabeled (i.e., natural abundance) silk fibroin sample is also shown.

DISCUSSION

The conformation of the silk II form, reported by Marsh et al. using X-ray diffraction analysis, has been established as an array of antiparallel β-sheets oriented such that the all of the Ala methyl groups and Gly residues face opposite sides, thus giving rise to a "polar-antiparallel" arrangement (*5*). A monoclinic unit cell was proposed where the chains in consecutive sheets are staggered when viewed along the intersheet distance. These general features have largely been supported by Fraser and co-workers (*6*) by an independent analysis of the X-ray diffraction patterns of an $(AG)_n$ model system, and the intersheet distances were further clarified by Lotz and Cesari (*11*, *12*). Therefore, to a first approximation, the amino acid sequence of the crystalline region comprising the β-sheet structure is an alternating sequence of Ala and Gly residues. Interestingly, a reexamination of the X-ray diffraction pattern of *B. mori* silk fibroin fiber by Takahashi et al. (*7*) revealed an "antipolar antiparallel" model, composed of antiparallel chains where the methyl groups of the Ala residues alternately lie on both sides of the β-sheet, since this refined model provided a "better fit" to the observed diffraction pattern. Fraser et al. (*6*) reported that the diffraction pattern of the crystalline Cp fraction (the precipitate obtained from an aqueous solution of fibroin treated with pancreatic chymotrypsin) was similar to that of powdered silk fibroin and to that of the model polypeptide $(GAGAGS)_n$ containing Ser residues. This finding is substantiated by our own studies (*32*) where we showed that the Ser residues act as a stabilizing entity of the basic $(AG)_n$ β-sheet structure through hydrogen bonding of the side-chain hydroxyl groups with carbonyl groups on adjacent chains.

The effect of individual amino acid residues on the conformational preferences within globular proteins has been extensively studied by a number of researchers (*38*). According to these studies, the distribution of Tyr residues is significantly below average in helical regions, and Tyr does

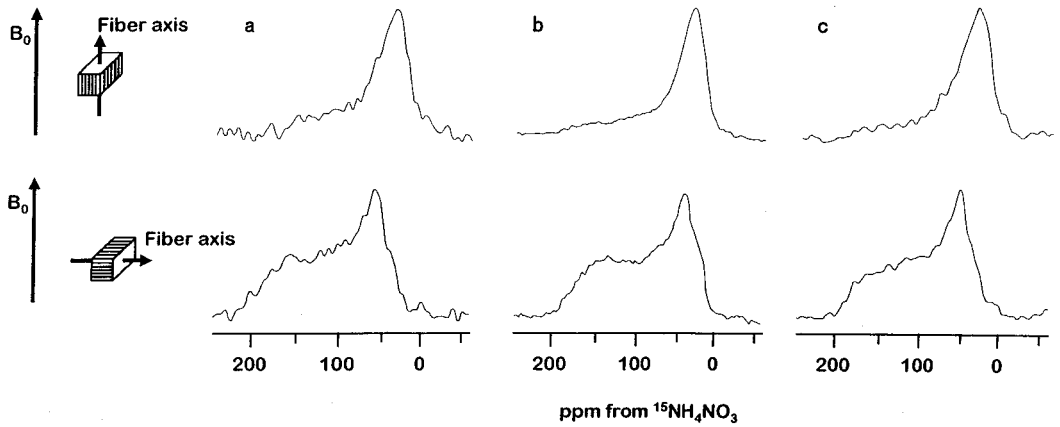

FIGURE 11: Solid-state ^{15}N NMR spectra (0−200 ppm) of the labeled, uniaxially aligned *B. mori* silk fibroin fiber: (**a**) [^{15}N]Tyr fiber, (**b**) [^{15}N]Val fiber, and (**c**) [^{15}N]Ser fiber. The fiber axis was placed parallel (upper spectra) and perpendicular (lower spectra) to the static magnetic field direction B_0. Approximately 30% of the intensity arising from nonoriented powder patterns was subtracted from the experimental spectra.

not exhibit a propensity for forming helical structures. Similarly, the distribution of Val residues was shown to be significantly above average in β-sheet regions. Hence, our findings substantiate the propensity of Tyr and Val residues in globular proteins, which is reported to be considerably higher for β-sheet structures (*39*, *40*).

Relatively few studies have reported on the structural behavior of the Tyr residue within *B. mori* silk fibroin. Using ^{13}C spin−lattice relaxation, the dynamic feature of the Tyr side chains in *B. mori* silk fibroin was investigated by Saito et al. (*41*). The dynamic behavior of the Tyr side chains in *B. mori* silk, reported by Kameda et al. (*31*) using solid-state ^2H NMR spectroscopy, revealed that [3,3-$^2H_2$]Tyr-labeled silk fibroins showed a typical rigid powder pattern, indicating that there is essentially no motion about the C_α−C_β bond axis, thereby revealing the existence of distinct rotameric populations within the oriented domains. On the contrary, the ^2H NMR spectra of silk fibers with ^2H-labeled aromatic rings, that is, [3′,5′-$^2H_2$]Tyr-labeled silk fibroins, exhibited two dynamic components. Here, the presence of a rigid powder contribution and a motionally averaged contribution indicated that some of the Tyr side chains are in fact mobile at the phenolic ring. This motion was characterized to be a π-flip, typical of aromatic rings. Moreover, the ^2H NMR line shape could be simulated by attributing 20% of the signal to a motionally averaged component with a fast rate of $\sim 10^6$ Hz, while the remaining 80% reflected a much slower component ($< 10^3$ Hz). To our knowledge, there has been no report on the dynamics of Val residue(s) in *B. mori* silk fibroin, yet.

An apparent pK_a value of ~10.1 for the phenolic hydroxyl group of Tyr in silk fibroin indicated a favorable deprotonation (*37*). This largely precludes the formation of hydrogen-bonding interactions involving the hydroxyl groups. The absence of hydrogen bonding is likely to promote the π-flip motions of the phenolic ring as revealed by our ^2H NMR study of [3′,5′-$^2H_2$]Tyr-labeled silk fibroin (*31*). Indeed, by enabling the π-flip motions to occur, the model proposed by Takahashi et al. (*7*), where the methyl groups of the Ala residues alternately point to either side of the sheet, is more feasible. The proposed antipolar-antiparallel arrangements of the fibroin chains are expected to bring relatively more local disorder in the stacking of sheets and, consequently, the bulky side-chain dispositions.

The driving force for self-aggregation of the fibroin molecules into a β-sheet structure is most likely a hydrophobic exclusion of the solvent by the $(AG)_n$ sequence, and the role of the Ser residue is presumably to stabilize the β-sheet structure through hydrogen bonding. The occurrence of bulky aromatic side chains of Tyr within the silk I structure possibly exerts a disruptive effect on the hydrophobic interactions between the basic $(AG)_n$ chains. Interestingly, our results show that the Tyr residues in the "oriented domains" of *B. mori* silk fibroin (silk II) are highly oriented in such a way that the ϕ, ψ torsional angles of this residue can easily accommodate a β-sheet conformation.

By comparing the ^{13}C NMR chemical shifts and the X-ray structures of proteins, Spera and Bax (*42*) and we (*27*) suggested that the $\Delta\delta$ values for the C_α and C_β resonances correlate quantitatively well with the backbone torsional angle obtained from the crystal structures. The ϕ and ψ values determined from the ^{15}N NMR experiments of silk fibroin are nicely consistent with the range predicted by the contour plots constructed from the observed ^{13}C chemical shifts of the C_α and C_β carbons of the Tyr residues in other proteins. However, the packing of the polypeptide chains into β-sheets in the vicinity of the Tyr residue is suggested to be less tight than around the Ser residues, probably due to the disordered side-chain orientations, described above (*7*). It is also worth mentioning that the diffuse streak scattering observed between the layer lines of the X-ray diffraction patterns by Takahashi et al. has been interpreted as arising from the periodic occurrence of the Ser residue within the β-sheet structure. Nevertheless, the presence of Tyr residues within the β-sheet structure may equally explain this effect.

CONCLUSION

The results of the present investigation have established that *B. mori* native silk fibroin can be successfully labeled biosynthetically at specific main-chain positions with [^{13}C]Tyr, [^{13}C]Val, [^{15}N]Tyr, [^{15}N]Val, and [^{15}N]Ser amino acids. The simple method can be extended to other related biological systems for site-specific labeling of particular residues in fibroin-like molecules for structural characterizations. Given that the repeated $(AG)_n$ sequence in the silk II form confers the basic β-sheet structure to *B. mori* silk fibroin, the role

of the short polar side chain of Ser is suggested to stabilize the β-sheet structure via side-chain to main-chain hydrogen bonding (*32*). Employing ^{13}C CP-MAS NMR, we have established that the bulky hydrophobic side chains of Tyr and Val may readily be included in the β-sheet structure of the *B. mori* silk fiber. Here, it appears that in the silk I form (and/or LiBr-treated samples) particularly the Tyr residues exhibit a larger distribution of their torsion angles (i.e., unordered structures), whereas in the silk II form the distribution is significantly restricted to an extended β-sheet conformation. The ^{13}C CP-MAS NMR analysis of the model peptides **1** and **2** also indicates that both the position and the relative content of Tyr in the $(AG)_n$ model system can be critical in causing the structural change from silk I to silk II, in a quantitative manner (unpublished data). A more systematic analysis of the simultaneous destabilizing effects, exerted by these residues on the silk I structure, is currently being analyzed in our laboratory with the help of designed model peptides. The current analysis also suggests that the ^{13}C NMR chemical shift values of the Tyr C_α resonance may be more sensitive to the backbone conformation accommodating the β-sheet structures, whereas the dependence of the Tyr C_β and Val C_α chemical shifts on the backbone conformation met with limited success. Finally, our experiments clearly indicate that a number of different solid-state NMR techniques are required to obtain detailed knowledge about the intra- and intermolecular conformational geometry, particularly in the case of fibrous proteins such as silk.

REFERENCES

1. Asakura, T., and Kaplan, D. L. (1994) in *Encyclopedia of Agricultural Science* (Arutzen, C. J., Ed.) Vol. 4, pp 1−11, Academic Press, New York.
2. Shimura, K. (1980) *Zoku Kenshi no Kozo* (Hojyo, N., Ed.) Shinshu University, Ueda.
3. Mita, K., Ichimura, S., and James, C. T. (1994) *J. Mol. Evol. 38*, 583−592.
4. Zhou, C., Confalonieri, F., Medina, N., Zivanovic, Y., Esnault, C., Yang, T., Jacquet, M., Janin, J., Duguet, M., Perasso, R., and Li, Z. (2000) *Nucleic Acids Res. 28*, 2413−2419.
5. Marsh, R. E., Corey, R. B., and Pauling, L. (1955) *Biochim. Biophys. Acta 16*, 1−34.
6. Fraser, R. D. B., and MacRae, T. P. (1973) in *Conformations of Fibrous Proteins and Related Synthetic Polypeptides*, Academic Press, New York.
7. Takahashi, Y., Gehoh, M., and Yuzuriha, K. (1999) *Int. J. Biol. Macromol. 24*, 127−138.
8. Konishi, T., and Kurokawa, M. (1968) *Sen'i Gakkaishi 24*, 550−554.
9. Okuyama, K., Takanashi, K., Nakajima, Y., Hasegawa, Y., Hirabayashi, K., and Nishi, N. (1988) *J. Seric. Sci. Jpn. 57*, 23−30.
10. Anderson, J. P. (1998) *Biopolymers 45*, 307−321.
11. Lotz, B., and Keith, H. D. (1971) *J. Mol. Biol. 61*, 201−215.
12. Lotz, B., and Cesari, F. C. (1979) *Biochimie 61*, 205−214.
13. Fossey, S. A., Nemethy, G., Gibson, K. D., and Scheraga, H. A. (1991) *Biopolymers 31*, 1529−1541.
14. Asakura, T., Kuzuhara, A., Tabeta, R., and Saito, H. (1985) *Macromolecules 18*, 1841−1845.
15. Saito, H., Tabeta, R., Asakura, T., Iwanaga, Y., Shoji, A., Ozaki, T., and Ando, I. (1984) *Macromolecules 17*, 1405−1412.
16. Asakura, T., and Yamaguchi, T. (1987) *J. Seric. Sci. Jpn. 56*, 300−304.
17. Ishida, M., Asakura, T., Yokoi, M., and Saito, H. (1990) *Macromolecules 23*, 88−94.
18. Nicholson, L. K., Asakura, T., Demura, M., and Cross, T. A. (1993) *Biopolymers 33*, 847−861.
19. Asakura, T., Aoki, A., Demura, M., Joers, J. M., Rosanske, R. C., and Gullion, T. (1994) *Polym. J. 26*, 1405−1408.
20. Asakura, T., Demura, M., Hiraishi, Y., Ogawa, K., and Uyama, A. (1994) *Chem. Lett.*, 2249−2252.
21. Asakura, T., Demura, M., Date, T., Miyashita, N., Ogawa, K., and Williamson, M. P. (1997) *Biopolymers 41*, 193−203.
22. Asakura, T., Minami, M., Shimada, R., Demura, M., Osanai, M., Fujito, T., Imanari, M., and Ulrich, A. S. (1997) *Macromolecules 30*, 2429−2435.
23. Demura, M., Minami, M., Asakura, T., and Cross, T. A. (1998) *J. Am. Chem. Soc. 120*, 1300−1308.
24. Asakura, T., Ashida, J., Yamane, T., Kameda, T., Nakazawa, Y., Ohgo, K., and Komatsu, K. (2001) *J. Mol. Biol. 306*, 291−305.
25. Asakura, T., Ashida, J., and Yamane, T. (2001) in *High-Resolution NMR Spectroscopy of Polymers*, American Chemical Society, Washington, DC (in press).
26. Asakura, T., Iwadate, M., Demura, M., and Williamson, M. P. (1999) *Int. J. Biol. Macromol. 24*, 167−171.
27. Iwadate, M., Asakura, T., and Williamson, M. P. (1999) *J. Biomol. NMR 13*, 199−211.
28. Ulrich, A. S., and Grage, S. L. (1998) in *Solid State NMR of Polymers* (Ando, I., and Asakura, T., Eds.) pp 190−211.
29. Kameda, T., and Asakura, T. (2001) in *Annual Report on NMR Spectroscopy* (Webb, G. A., Ed.) Academic Press, London (in press).
30. Saito, H., Tabeta, R., Kuzuhara, A., and Asakura, T. (1986) *Bull. Chem. Soc. Jpn. 59*, 3383−3387.
31. Kameda, T., Ohkawa, Y., Yoshizawa, K., Nakano, E., Hiraoki, T., Ulrich, A. S., and Asakura, T. (1999) *Macromolecules 32*, 8491−8495.
32. Kameda, T., Ohkawa, Y., Yoshizawa, K., Naito, J., Ulrich, A. S., and Asakura, T. (1999) *Macromolecules 32*, 7166−7171.
33. Asakura, T., Sakaguchi, R., Demura, M., Manabe, T., Uyama, A., Ogawa, K., and Osanai, M. (1993) *Biotechnol. Bioeng. 41*, 245−252.
34. Panitch, A., Matsuki, K., Cantor, E. J., Cooper, S. J., Atkins, E. D. T., Fournier, M. J., Mason, T. L., and Tirrell, D. A. (1997) *Macromolecules 30*, 42−49.
35. Asakura, T., Watanabe, Y., and Itoh, T. (1984) *Macromolecules 17*, 2421−2426.
36. Asakura, T., Yoshimizu, H., and Yoshizawa, F. (1988) *Macromolecules 21*, 2038−2041.
37. Asakura, T., Watanabe, Y., Uchida, A., and Minagawa, H. (1984) *Macromolecules 17*, 1075−1081.
38. Richardson, J. S., and Richardson, D. V. (1990) in *Prediction of Protein Structure and the Principles of Protein Conformation* (Fasman, G. D., Ed.) pp 1−98, Plenum Press, New York.
39. Minor, D. L., Jr., and Kim, P. S. (1994) *Nature 367*, 660−663.
40. Kim, C. A., and Berg, J. M. (1993) *Nature 362*, 267−270.
41. Saito, H., Ishida, M., Yokoi, M., and Asakura, T. (1990) *Macromolecules 23*, 83−88.
42. Spera, S., and Bax, A. (1991) *J. Am. Chem. Soc. 113*, 5490−5492.

BI0119013